(2)

FTD-ID(RS)T-0022-89

FOREIGN TECHNOLOGY DIVISION

JOURNAL OF CHINESE SOCIETY OF ASTRONAUTICS

(Selected Articles)

Approved for public release;
Distribution unlimited.

HUMAN TRANSLATION

FTD-ID(RS)T-0022-89 24 May 1989

MICROFICHE NR: FTD-89-C-000366

JOURNAL OF CHINESE SOCIETY OF ASTRONAUTICS
(Selected Articles)

English pages: 36

Source: Yuhang Xuebao, Nr. 2, 1988, pp. 47-52; 81-87; 88-93

Country of origin: China
Translated by: Leo Kanner Associates
F33657-88-D-2188
Requester: FTD/TQTRE/Capt Adams

PREPARED BY:

TRANSLATION DIVISION
FOREIGN TECHNOLOGY DIVISION
WPAFB, OHIO.

TABLE OF CONTENTS

GRAPHICS DISCLAIMER

All figures, graphics, tables, equations, etc. merged into this translation were extracted from the best quality copy available.

JOURNAL OF CHINESE SOCIETY OF ASTRONAUTICS.

RESEARCH ON DISTRIBUTION OF SIZE AND AGGREGATE STATES OF BURNING ALUMINUM DROPLETS IN PROPELLANT COMBUSTION

Guo Shen (North China University of Technology)
Li Shufen (University of Science and Technology of China)

Abstract

This paper discusses the size and distribution of burning aluminum droplets during the combustion of aluminized propellant, as well as the influence of the size of the oxidizer grains and aluminum grains on aluminum agglomeration. Experimentation demonstrates that the aluminum agglomeration during burning of propellants composed of coarse oxidizers is very apparent, and also that fine aluminum agglomerates more readily than coarse aluminum in propellants with correspondingly coarse oxidizers. Experimental results support the "pocket model" of aluminum agglomeration in composite propellant. This paper, in addition, gives the results of microphotodensity analysis of the agglomeration combustion mechanism of aluminum: There are three different types of photodensity distribution curves, which we call the droplet type, mini-droplet type, and liquid-vapor transition type. Each represents an aggregate state of aluminum. Further, there is another type in which no aluminum streaks appear on the photographic plate, which we call the vapor-phase type. The combustion efficiency of aluminum rises throughout the above sequence, from droplet to vapor-phase type.

Key Terms: Aluminum propellant, composite propellant, combustion property of propellant, aluminum, agglomeration, macrophotography.

1. Foreword

Aluminum powder has become an important component of solid propellants; its purpose is to improve performance and control unstable combustion at various frequencies. Aluminum powder additives are thus obviously able to effect a change in certain combustion characteristics, having an effect on the speed of combustion, the agglomerative products, the combustion stability and other areas of interest. Much has been written to confirm the fact that aluminum can accumulate and agglomerate on the fuel surface during the process of combustion [1-5], a point which is very important in actual use. Because

---

Translator's Note: For bibliography, see page 11.

four important characteristics of an engine -- combustion efficiency, specific impulse efficiency, sound vibration control capacity, residue accumulation -- have connections with the combustion speed of aluminum droplets, they are also involved with the degree of agglomeration of aluminum.

It has already been experimentally verified that when the metal component is too high, the specific impulse of aluminum propellant is much lower than the theoretically calculated values. The reason for this discrepancy is that a chemical equilibrium among the components has not been achieved, and that a balance of speed between the combustion products of aluminum and the vapors which have been exhausted through the nozzle has not been realized (that is, because of the problem of speed retardation). The published material [5] has already dealt with mathematical functions relating aluminum drop agglomeration size, air flow speed produced by propellants, and aluminum droplet speed.

The size of agglomerative aluminum droplets in the process of combustion is a very good measure of the degree of agglomeration of aluminum; at the same time, it is also an important parameter for calculating the flow loss. Photography is one of the effective methods for measuring the size of burning aluminum droplets, but this method is likely to suffer the interference of the diffuse flame produced by the aluminum droplets themselves. For this reason, the bright region of aluminum droplet combustion on the photograph by no means represents its actual size, as has been pointed out by many foreign scholars [1,2,6]. So how is it possible to determine the actual size of a burning aluminum droplet? What relationship do their aggregate state and combustion mechanism show? And so on. These problems have attracted the attention of scholars both here and abroad.

This paper offers techniques based on macrophotography and microphotodensity analysis for measuring the size of burning aluminum droplets, and undertakes a semi-quantitative investigation of the influence of the grain size of oxidizers and aluminum on the degree of agglomeration. At the same time, it also studies the aggregate state of burning aluminum

droplets.

2. Experimentation

A. Experimental Apparatus

Experimentation was undertaken in a pressurized combustion chamber with two transparent observation windows. We used the model KD-4203 macrophotographic apparatus developed by our group for single-width photographs of the entire flame region of combustion, and used a model MD-100 microphotodensity apparatus (Zeiss/Jena) with an automatic recorder for photodensity analysis on the negative.

B. Test Sample

We tested four propellants, with a basic composition of 69% oxidizer, 14% cohesive ingredient, 14% aluminum powder, and 3% other additives. Changes to the sizes of oxidizer and aluminum grains were undertaken as shown in on the left side of Table 1.

Table 1.

Propellant Number	Nom. Diameter (μm)		Pressure (Pa)							
	Oxidizer	Aluminum	$1x10^6$		$3x10^6$		$5x10^6$		$7x10^6$	
			A	B	A	B	A	B	A	B
I	~360	7-8	200	300	400	480	210	330	310	350
II	~360	~50	130	190	110	200	110	160	160	190
III	~5	7-8	C							
IV	~5	~50	50	-	50	-	C			

A. Size of 50% of total of burning aluminum droplets (μm).
B. Average size (μm).
C. Aluminum streaks not observed.

C. Measurement Methods

The type of macrophotography used was of the single-width class. Although it has only the capacity to record a given instant of a process, if a sufficient number of exposures are made under the same experimentational conditions, and if instants of stable combustion are chosen for the exposures, the results may be considered representative. The exposure time for macrophotography is generally longer than for high-speed photography, and for this reason each burning aluminum droplet, as it moves, is recorded as a streak on the negative, with the width of the streak indicating the size of the aluminum droplet.

For bright streaks with an obvious "core," the photodensity scanning graph is relatively regular (as the "→" in Fig. 1 shows); by measuring the

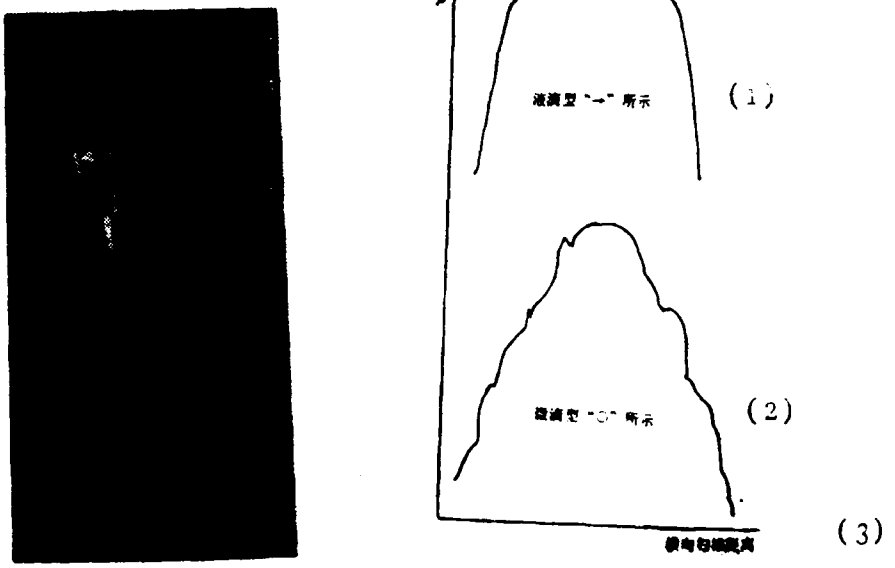

Fig. 1. Photograph of flame of sample II burning under 1×10^6 Pa pressure, and graph of aluminum droplet microdensity. Key: (1) droplet type, marked "→" on photograph; (2) mini-droplet type, "○" on photo; (3) crosswise scanning distance.

shoulder width of this scanning graph, and passing it through the scanning scale conversion, it is possible to obtain the width of the streak's "core" and equate this with the size of the burning aluminum droplet. For finding the width in the case of streaks that have no obvious core, it is only possible to employ an approximation method, based on simulation involving photographic measurement of the width of the light emitted from a glowing metal thread.

3. Results and Discussion

A. The Two Types of Aluminized Propellant Flames

The combustion of composite aluminized propellant occurs in two different kinds of visible flames. The characteristic of the first kind of flame is that on the photograph one can only see a flame of a well-distributed brightness, but not streaks of burning aluminum droplets, as the photograph of the combustion flame of propellant III in Fig. 2 shows. Burning aluminum droplets appearing as a locus of bright stripes on the photograph characterize the second type of flame, as shown in Fig. 1. When propellant I and II burn in the $1x10^6$ to $7x10^6$ Pa pressure range, they both exhibit this kind of flame.

Fig. 2. Photograph of flame of sample III burning under $1x10^6$ Pa pressure.

The appearance of two different types of flame is most importantly a result of the difference in oxidizer grain size and aluminum grain size in the propellant, but experimentation has discovered that a critical range of pressure exists in which the two types of flame can be converted from one to the other. When propellant III burns at less than $5x10^5$ Pa pressure, the probability of the appearance of aluminum streaks is 50%. When the pressure is reduced to $3x10^5$ Pa, not only do countless aluminum streaks appear, but also a

considerable portion of them has a size far larger than the oxidizer and aluminum grains, as Fig. 3 shows. At this time there is a transformation from

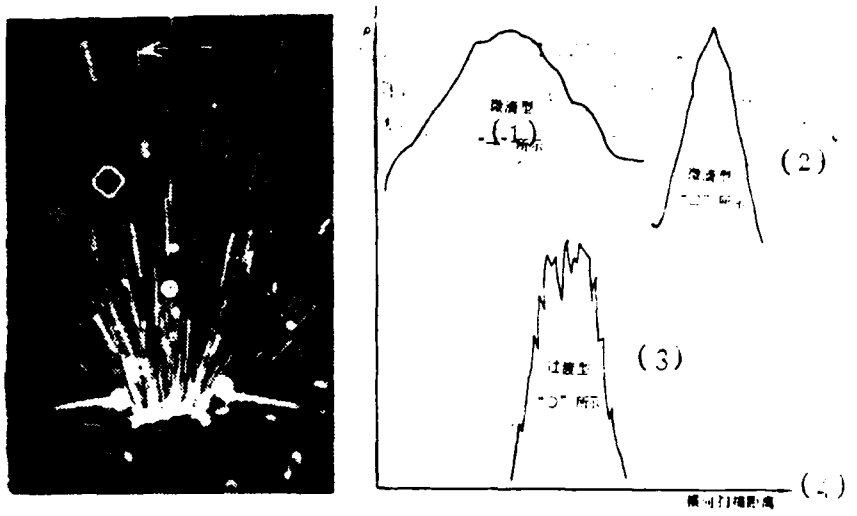

Fig. 3. Photograph of flame of sample III burning under $3x10^5$ Pa pressure, and graph of aluminum droplet microdensity. Key: (1) mini-droplet type "→"; (2) mini-droplet type "□"; (3) transitional type "○"; (4) crosswise scanning distance.

flame type one to flame type two. Propellant IV, at or below $3x10^6$ Pa pressure, shows clear aluminum streaks; but when the pressure is increased to $5x10^6$ Pa, the streaks basically no longer appear, the conversion being from flame type two to type one. When propellants I and II are burned at $7x10^6$ Pa pressure, aluminum streaks still appear; because of limits on the conditions, experimentation has not been possible under higher pressures and the critical pressure range has not yet been discovered.

B. Measuring Aluminum Streak Photodensity and Burning Droplet Aggregate State

When the photographic method is used to record the dynamic process of burning aluminum droplets in aluminized propellant, black streaks appear in the negative. Applying microphotodensity calculations to the streaks on the negative to undertake crosswise photodensity scanning obtains results that show that all of the streaks have one photodensity distribution, but their

form may not be the same, as in Fig. 1 and 3. By far the greater number of streaks has an even brighter "core"; or, put another way, a bright "core" is surrounded by an area of low light density. The size of this core is the actual size of the above mentioned burning aluminum droplets. It is necessary to point out that if some burning aluminum droplets are surrounded by the basic flame of the propellant, the measurement of photodensity suffers interference. Nevertheless, under ordinary circumstances, the light density of the "core" is greater than that of the surrounding flame, so that the size of the "core" and the aggregate state can still be read.

On the basis of over 1,000 photodensity distribution graphs, it can be said that they reflect different aggregate states of burning aluminum droplets, which basically can be classified into three groups. For the sake of clarity, we will call these groups the "droplet type," the "mini-droplet type," and the "liquid-vapor transition type."

The droplet type: The characteristic of this type of photodensity graph is that it has a broad plateau, as the "→" in Fig. 1 shows; the plateau indicates that the brightness is evenly distributed. Some graphs are irregular on the two sides, or the height of their plateau is relatively low, or there appear on the plateau pulses with relatively high "frequency" but low "amplitude." These may be considered cases of interference from the propellant's basic flame; or they may have been caused during the photographic process by deviation from the plane of focus. Even though this is the case, the plateau still can be recognized, as Fig. 4 shows; but for the aluminum droplets that deviate severely from the plane of focus, size measurement is without significance.

On the basis of the gaseous state combustion mechanism of aluminum, this sort of photodensity distribution graph reflects the fact that an aluminum droplet that has been ignited both vaporizes and also burns. For this reason, in its vicinity there forms a region composed of vapors in the process of burning and scorching hot combustion products. This aluminum droplet that has ignited is what we called above the "even brighter core in a bright region."

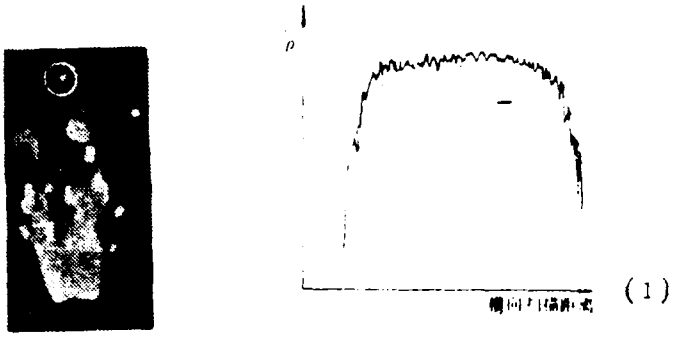

Fig. 4. Photograph of unfocused flame and aluminum droplet microphotodensity distribution graph. Key: (1) Crosswise scanning distance.

Ordinarily, it is far larger than the original aluminum grain in size; it corresponds to the plateau portion of the photodensity graph. Under these conditions, whether because the droplet is excessively large, or whether because the heat that is transmitted from the outer portions of the droplet is not sufficient, there occurs a situation in which a droplet cannot instantaneously vaporize. For this reason a relatively large, well-distributed center of luminescence is recorded by the photograph.

The mini-droplet type: The graph in Fig. 3 marked by "□" is a typical example of the mini-droplet photodensity graph. It shows a very small aluminum point of luminescence. This has no basic difference with the droplet type, just that its "core" is very small.

The liquid-vapor transitional type: The graph marked by "○" on Fig. 3 is representative of this kind of graph. Its characteristic is that the entire graph is formed of very many mutually linked small peaks. This may be because the aluminum droplet is placed in conditions promoting vaporization, but it has not, at the time immediately following ignition, thoroughly vaporized. For this reason, once ignition takes place, it is split into very many droplets (but much smaller than those of the mini-droplet type). Immediately following vaporization, the droplets are burned. At this time they are unable to spre ł out and become individual luminescence centers. For this reason, on the photograph is recorded a "even brighter core" formed of

very many closely linked small luminescence centers surrounded by a misty cloud-form, low-luminescence region.

Vapor type: Our paper has mentioned that in the first kind of flame aluminum streaks do not appear. This is explained by the fact that aluminum powder in propellants basically has not produced obvious agglomeration, and furthermore, near the combustion surface, there is complete vaporized combustion. For this reason, it is called the vapor type.

Thus the combustion of aluminum in composite aluminized propellant takes place in four different kinds of aggregate states. These states are the droplet type, the mini-droplet type, the liquid-vapor transitional type, and the vapor type. The first three aggregate states' external characteristic is that streaks appear on the photograph. Obviously, the combustion rate increases in the order listed above.

The aluminum streaks that are produced when propellant IV is burned at pressures equal to or below 3×10^6 Pa, as in shown when their photodensity is measured, for by far the most part, belong to the mini-droplet and transitional types; but they also include a small number of droplet types. This is to say, an increase in pressure during combustion is favorable for the vaporization of aluminum and causes the burning aluminum droplets' aggregate state to tend toward the vapor type. From the macroscopic point of view, it is conducive to the transformation from the second type of flame to the first type. On the other hand, as the pressure at the time of combustion is reduced, agglomeration of aluminum is easily produced. Propellant III can also show droplet types of aluminum streaks, that is, change from type one flame to type two flame. In the photodensity distribution graph for propellants I and II, all three types are present, and, comparably speaking, the droplet type is somewhat more common, the transitional type is somewhat rarer.

C. Size Distribution of Burning Aluminum Droplets

Based on the measurement of photodensity and simulated experiments concerning glowing metal wires, a study has been undertaken of the size distribution of aluminum droplets on the combustion surface. From considerations of the random nature of the photography and the uneven distribution of composite propellant, statistical calculations were made for the size of the burning aluminum droplets from ten negatives for each sample at each pressure increment, and an aluminum agglomerate drop size distribution graph was obtained. A relative comparison was made of different propellants' agglomerative degree using the "largest size corresponding to the 50% of the total of aluminum streaks" and the "mean size of all of the aluminum streaks." Figure 5 is the aluminum droplet size distribution graph of propellants I and II when burned under a pressure of 5×10^6 Pa. In the distribution graphs for other pressures the size distribution graph slope for propellant II is greater than that for propellant I.

This kind of measurement does not consider the transitional type. The reason for this is that, speaking from the point of view of the inferred mechanism, they no longer have a "core"; furthermore, there is no way to find the width of the plateau from the density distribution graph.

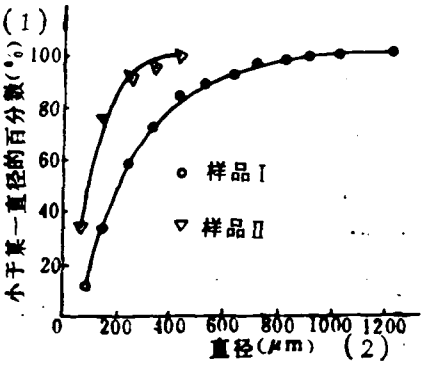

Fig. 5. Aluminum droplet size distribution for samples I (○) and II (▽) burning under 5×10^6 Pa. Key: (1) percentage smaller than given size; (2) size (μm).

On the basis of the density distribution graphs discussed above and the calculated results, it is possible to obtain the experimental results shown in Table 1. From these results it is possible to make the following

observations. (1) Within the range of ordinary working pressure, propellants I and II, composed of coarse oxidizers, when burned, more easily produce the phenomenon of aluminum agglomeration than do propellants III and IV, which have fine oxidizers. (2) Propellant I, which has a coarse oxidizer and fine aluminum powder, has a degree of agglomeration that is greater than propellant II, which is composed of coarse oxidizer and coarse aluminum powder.

These experimental results coincide with the results obtained from our organization's color line shadow experiments and laser shadow experiments. They are also uniform with the "pocket model" for aluminum agglomeration in propellants proposed by Cohen [7]. Using the Beckstead experimental formula proposed by King [8] to calculate the aluminum agglomeration size of the above four propellants, the results are again basically the same as for our experiment.

Thanks to our colleague Liu Wei for participation in this experimentation.

BIBLIOGRAPHY

1. Hartman, K.O. "Combustion kinetics of aluminum particles in propellant flames," WSS/CI paper, 71-24, Apr. 1971.

2. Diloreto, V.D. and D.W. Netzer. "An experimental study of solid propellant defulgration using high speed motion picture and postfire residue analysis," AD/AO 92423, 1980.

3. Povinelli, L. and R.A. Rosenstein. "Alumina size distributions from high-pressure composite solid-propellant combustion," AIAA paper, No. 64-115, Jan. 1964.

4. Price, E.W., R.K. Sigman and J.K. Samabamurthi. "Behavior of aluminum in solid propellant combustion," AD/AO 52492, 1977.

5. Watermeier, L.A., W.P. Aungst and S.P. Pfaff. Ninth Symposium (International) on Combustion, Academic Press, 1963, p. 316.

6. Wood, W.A. Progress in Astronautics and Rocketry, Vol. 1, Solid Propellant Rocket Research, Academic Press, 1960, pp. 287-291.

7. Cohen, N.S. "A pocket model for aluminum agglomeration in composite propellants," AIAA paper, No. 81-1585, July 1981.

8. King, M.K. "Predicted and measured effects of pressure and crossflow velocity on composite propellant burning rate," AD-A098090.

THE EROSIVE BURNING CHARACTERISTICS OF ALUMINIZED HIPB COMPOSITE PROPELLANT "87"

Xia Xiang Xing, Man Jia Zhu, Li Shui Chi, Li Yi Min
(Beijing Institute of Aeronautics and Astronautics)

Abstract

This paper reports on the experimental investigation of erosive burning for composite propellant "87" using the method of slab motor interrupted burning. The semiempirical relations of the erosion ratio as a function of combustion gas velocity and pressure are established, and analysis is performed. The data obtained by experimentation are reasonable, and show that this kind of method can be used for relatively high-temperature combustion and soft composite propellants.

Key Terms: Aluminized propellant, hydroxy terminated polybudiene propellant, erosive burning, combustion property of propellant.

1. Foreword

China's propellant "87" is a kind of aluminized ammonium perchlorate composite propellant. It uses hydroxy terminated polybudiene as its cohesive component. Its specific impulse is relatively high, and its mechanics performance and technological nature rank high among propellants. It is a propellant that in recent years has been used relatively frequently.

When designing high-performance solid-fuel rocket motors, in planning the charge and calculating and internal trajectory capabilities, it is necessary to control the propellant's erosive burning characteristics. We have undertaken an experimental investigation of the erosive characteristics for composite propellant "87."

Translator's Notes:
Note in original: Paper received 8/29/86.
For bibliography, see page 24.
In the translation, underlining in subscripts and superscripts represents italics in the original.

"Erosive burning characteristics" refers to the relation of the combustion speed r with the combustion gas crosswise rate of flow u, and the pressure p. This is ordinarily expressed by the erosion ratio ε ($\varepsilon=r/r_0$, with r_0 the base non-erosive burning speed) considered as a function of u and p. It is also called the erosion function.

Because erosive burning is a complicated physical and chemical process, although there have been proposed many theoretical models for erosive burning, nevertheless these models cannot yet be used directly in quantitative predictions of the erosive burning characteristics. The result is that in the development of motors the empirical method is still relied upon to establish the erosion function.

2. Experimental Investigation Methods

The interrupted burning method has been widely used in the experimental investigations of double-base propellant erosive burning. It does not require special equipment. The experimental components can be directly examined after interruption so that conditions during the process of combustion can be investigated. For this reason it is quite convenient to use. Nevertheless, if the combustion temperature of the composite propellant is very high and its strength is relatively low, transformation can occur and the interruption is relatively difficult. It is not easy to maintain the charge in a complete state. On the basis of the characteristics of composite propellant and in accordance with our analysis of currently possible experimental methods, we have developed a kind of slab motor interruption burning method. This method utilizes two slab-shaped charges for burning in the motor. Direct measurement of the combustion thickness of the slabs after interruption of burning establishes the erosive combustion. In the passage between the slabs, the rate of flow of combustion gases along the axis undergoes great changes; in one experimental run it is possible to obtain many sets of data, and it is at the same time possible to measure the distribution of pressure p along the passage. For this reason it is possible to establish reliably the relationship of the erosive combustion rate of burning speed r with u and p.

A. The Experimental Motor

As Fig. 1 shows, the motor is composed of a head piston, housing, charge, and nozzle. The piston, at the head, is joined by a dowel to the

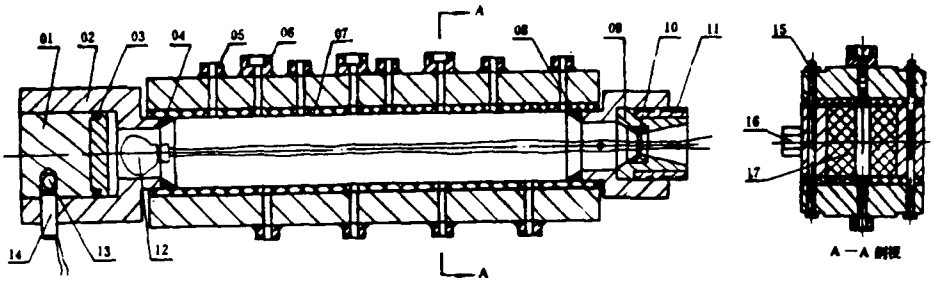

Fig. 1. Experimental motor. Key: (01) piston; (02) housing; (03) seal; (04) forward transitional section; (05) water hole; (06) pressure measuring hole; (07) fireproofing layer; (08) rear transitional section; (09) nozzle; (10) graphite lining; (11) fitted screw cap; (12) ignition powder pack; (13) interruption powder pack; (14) dowel; (15) bolt assembly; (16) pressure measuring hole; (17) charge.

housing. On the housing are affixed, on opposite sides, two rectangular charge slabs, each forming virtually a two-dimensional combustion chamber. Only the side of the slab facing the passageway burns; the other five sides are enclosed by an fireproof layer. Between the two slabs a certain distance is maintained, forming a combustion vapor passageway that is rectangular in section. On the other two sides of the passageway, two cover plates are closely fitted. On the cover plates, along the axis of the passageway, is set up a row of tubes for measuring pressure and for waterspouts. In the former are installed sensors; the latter are used during interruption of burning, spouting out cooling water into the combustion chamber. The motor's nozzle is a Lawaer nozzle inlaid with a lining of graphite.

When the slab has burned to a preset time, the dowel is knocked out by the interruption powder pack igniting; at the same time the piston is knocked out by the high pressure combustion gases in the combustion chamber. The pressure in the combustion chamber swiftly decreases, the burning of the slabs is interrupted, and the cooling water immediately is forced out in great

quantities into the combustion gas passage and prevents the slabs from reigniting. The injection of the cooling water is automatically controlled by a single transport system.

B. Measurement

When the slab charges burn, the rate of flow of combustion gas in the passageways along the axis gradually increases, reaching its greatest speed at the exit. The static pressure of the combustion gas along the axis shows some decrease, and for this reason the charge on each section burns at a different speed. Only by actual measurement can the pressure, rate of flow, and change in combustion speed along the axis be determined; only in this way can a formula for the erosive characteristics of the slab be determined. Our experimental motor has five pressure-measuring holes along the combustion gas passage, set up at certain intervals. At the entrance to the nozzle there is also one other pressure-measuring hole. They are joined by a pressure sensor and a sixteen-line oscillator. From one experiment it is possible to obtain six p-t graphs (Fig. 2), and afterwards transform them to p-x graphs (Fig. 3), showing the change in pressure in the combustion gas chamber along the axis.

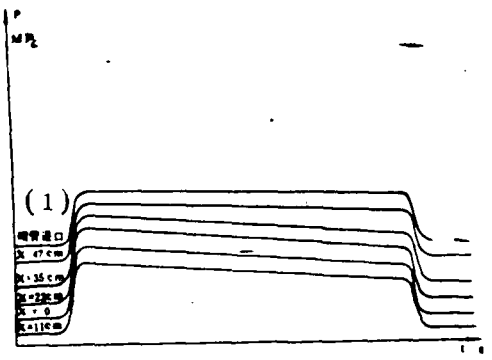

图2 一次试验的六条$p-t$线曲

Fig. 2. Six p-t curves from one experiment. Key: (1) nozzle mouth.

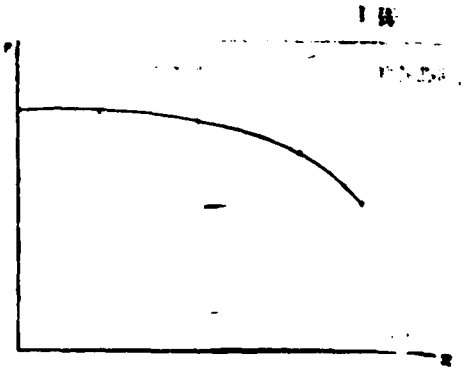

图3 通道内$p-x$曲线

Fig. 3. Curve p-x within the passageway.

The thickness of the slabs, or the distance between the charges affixed to the motor (the width of the passageway), was measured before and after burning. This makes it possible to establish the burning thickness Δ_e at different axis positions x, and to obtain the actual burning rate at each position, as:

$$r = \frac{\Delta e}{\Delta t} \tag{1}$$

In this formula, Δ_t is the combustion time, obtained from the graph p-t.

The area of a section of the passageway is obtained using the distance between the charges and the width of the passageway. The mean section area for each position in the passageway is given as:

$$A_p = \frac{1}{2}\,(A_{p_0} + A_{p_1}) \tag{2}$$

in which A_{p0} and A_{p1} are the passageway section areas before and after burning, respectively.

The rate of combustion gas flow at each section is indirectly established from the calculations given below.

Mass flow rate:
$$m = \int_0^x \rho_p r \Pi \, dx \tag{3}$$

Section density flow:
$$\rho u = m / A_p \tag{4}$$

By the formula for the increasing mass flow energy and the assumption of an equal section passageway, the combustion temperature at each section is calculated:

$$T = T_0 / \left[1 + \left(\frac{p_0}{p} - 1\right)\frac{k-1}{2k}\right] \tag{5}$$

The equation for this condition is:

$$\rho = p / RT \tag{6}$$

From the result of formulas (4) and (6), the combustion gas rate of flow is calculated:

$$u = (\rho u)/\rho \tag{7}$$

In the above formulas, ρ_{p} is the density of the propellant, Π is the length of the combustion periphery (that is, the width of the two slabs), ρ is the density of the combustion gases, p_0 and T_0 are respectively the pressure and temperature at the front end of the passageway. k is the specific heat ratio.

C. Range of Experimental Parameters

To expand the range of the experimental parameters, it was necessary to make changes in the pressure and the passageway exit rate of flow for each run of the experiment. Because the combustion area of the slabs do not basically change, we mainly relied on variations in the area of the nozzle throat section A to provide different experimental pressures. By changing the thickness of the slabs to change the section area of the combustion gas passageway and to obtain different exit rates of flow, we were able to achieve the goal of establishing the relation of ε with r under a relatively great range of values for p and u. The range covered includes p=3.43-11.08 MPa.

In this range, the pressure at the head is p_0=3.92-11.98 MPa.

The maximum value of the instantaneous exit rate of flow can reach 9000 m/s. The mean rate of flow in the passageway during experimentation was u=0-500 m/s.

The selection of the duration of combustion, Δt, was based on two considerations: The first is, it should not be too long, to avoid a change in A_p occasioned by the burning process, thus bringing about an increased deviation affecting the parameters. The second is, it should not be too short, which would cause an increase in the portion of Δt occupied by the time of increasing pressure. In our apparatus we also needed to guarantee the minimum time needed for the injection of the cooling water. The times selected for these experiments were Δt=0.100-0.200 s, with the majority controlled in the range 0.140-0.150 s.

3. Erosion Burning Characteristics

A. Most Important Propellant Parameters

It can be seen from Table 1 that 87-1 is a propellant with a mid-range combustion speed, and 87-2 is a propellant with a low-range combustion speed.

Table 1.

Propellant	Density g/cm²	Burning Temp., K	Spec. Heat Ratio	Molec.Wt., mol	Basic Burning Rate (Combust. Rate Device) 20°
87-1	1.741	3455	1.18	28.5	$r_0=0.6247\ p^{0.356}$ cm/s (p=5.88 MPa, r_0=1.174 cm/s)
87-2	1.740	3300	1.19	27.4	$r_0=0.2022\ p^{0.484}$ cm/s (p=5.88 MPa, r_0=0.477 cm/s)

B. *Non-erosive Combustion Speed* r_{m0} in the Experimental Motor

The conditions under which the charge burns in the experimental engine are not the same as those in the combustion rate device; nor, under the effect of non-erosive gas flow, is their basic combustion rate the same. For this reason, in order to analyze accurately and reliably the influence of erosive airflow on the charge combustion rate r, it was necessary to find the basic burning rate r_{m0} under non-erosive conditions. We used the interrupted burning method with the slab and at rates of flow that did not produce erosion we established the relation of r_{m0} and p. When the rate of flow of combustion gas was very low, u has no influence on r. The combustion rate at this time is the non-erosive combustion rate. From experimentation we obtained:

87-1 $r_{m0}=0.7443p^{0.3115}$cm/s (20°C)

87-2 $r_{m0}=0.3107p^{0.3411}$cm/s (20°C)

Comparing these with the combustion rate device in Table 1, we have:

87-1 $r_{m0}/r_0 = 1.1915 p^{-0.0433}$ (20°C)

87-2 $r_{m0}/r_0 = 1.5366 p^{-0.1419}$ (20°C)

In the range p=3.43-11.08 MPa, the non-erosive combustion flow in the experimental motor was somewhat larger than in the combustion rate device. In the case of propellant 87-1, it was approximately 7-13% larger; in the case of propellant 87-2 it was 9-27% larger. This corresponds with the general pattern. It is also possible to see that, the lower the pressure, the greater the deviation between r_{m0} and r_0. On the other hand, the higher the pressure, the greater the tendency of r_{m0} and r_0 to be comparable.

C. The Relations of Erosion Characteristics

For each experiment there were set up 14 measuring points at specific increments along the axis of the charge. After the experiment it was possible to obtain 14 sets of data for p, u and ε. For typical data see Tables 2 and 3; for the corresponding graphs see Fig. 4 and 5.

Eight experiments for propellant 87-1 and 14 experiments for propellant 87-2 provided over 100 sets of data each.

On the basis of the fluctuation patterns in the experimentally obtained $\varepsilon = f(p, u)$, we used $\varepsilon = 1 + K_1 p^{K_2} (u - u_{th})^{K_3}$, in which K_1, K_2, and K_3 are constants, u_{th} is the limiting rate of flow for the erosive burning that occurred. Manipulating the above formula, we obtain:

$$L_0(\varepsilon - 1) = L_0 K_1 + K_2 L_0 p + K_3 L_0 (u - u_{th})$$

This is a dual regression equation in which ε, p, and u are experimentally obtained data. Thus, from the regression formula it is possible to solve for K_1, K_2, and K_3. The final formula showing the semi-empirically obtained relations for erosive burning characteristics are:

87-1 $\varepsilon = 1 + 5.4474 \times 10^{-5} p^{0.73} (u - u_{th})^{1.26}$ $(u \geq u_{th})$

87-2 $\varepsilon = 1 + 28.361 \times 10^{-5} p^{0.49} u^{1.3}$

Table 2. Data for 87-1 (set 21)

p (MPa)	10.35	10.35	10.35	10.35	10.35	10.32	10.30	10.27	10.24	10.18	10.11	10.01	9.80	9.78
u (m/s)	0	8.7	15.6	36.4	60.0	89.4	105.4	123.9	145.0	171.2	201.8	232.6	267.0	286.8
ε_{actual}	1.000	0.997	0.994	1.000	0.997	1.011	1.038	1.042	1.068	1.110	1.166	1.252	1.365	1.413
ε_{calc}*	1.000	1.000	1.000	1.000	1.000	1.011	1.030	1.058	1.096	1.145	1.210	1.280	1.361	1.410
$(\varepsilon_{actual}-\varepsilon_{calc})/\varepsilon_{calc}$ (%)	0.0	−0.3	−0.6	0.0	−0.3	0.0	0.8	−1.5	−2.6	−3.3	−3.8	−2.2	0.3	0.2

*$\varepsilon_{calc}=1+5.4474\times10^{-5}\times p^{0.73}/(u-u_{th})^{1.36}$

Table 3. Data for 87-2 (set 34)

p (MPa)	4.89	4.89	4.89	4.89	48.8	4.88	4.88	4.86	4.83	4.80	4.75	4.68	4.58	4.52
u (m/s)	0.0	3.0	10.0	26.9	62.1	93.3	113.0	133.1	156.6	186.2	211.8	264.2	313.0	344.0
ε_{actual}	1.000	0.956	0.966	1.072	1.066	1.175	1.252	1.317	1.498	1.618	1.749	1.965	2.178	2.330
ε_{calc}*	1.000	1.000	1.000	1.000	1.132	1.224	1.286	1.386	1.438	1.546	1.643	1.851	2.050	2.176
$(\varepsilon_{actual}-\varepsilon_{calc})/\varepsilon_{calc}$ (%)	0.0	−4.6	−3.5	6.7	−4.4	−4.3	−2.7	−2.9	4.0	4.4	6.6	7.2	5.9	6.1

*$\varepsilon_{calc}=1+28.361\times10^{-5}p^{0.49}u^{1.3}$

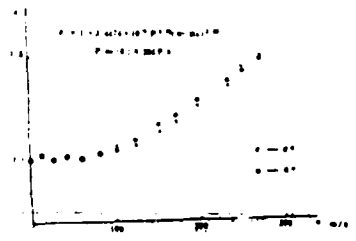

Fig. 4. One set of experimental data for 87-1.

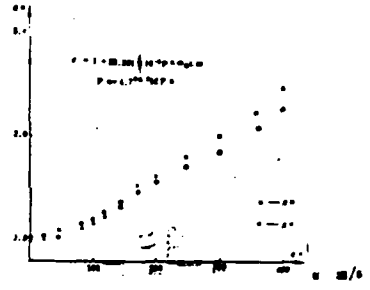

Fig. 5. One set of experimental data for 87-2.

In the formula, the units for p are MPa, the units for u are m/s.

Using this formula for calculation we obtain a comparison between ε_{calc} and ε_{actual} (Table 2, Table 3).

D. Limiting Rate of Flow u_{th} for the Occurrence of Erosion

From experimentation it appears that the influence of the combustion gas rate of flow on the burning speed of the slabs does not exist constantly from the beginning, but only appears when the rate of flow has increased to a certain value. The rate of flow at this time is called the limiting rate of flow u_{th}. When $u<u_{th}$, the value of u does not influence ε. When $u\geq u_{th}$, the erosion effect is produced, with $\varepsilon\geq 1.0$.

This experiment shows that in the case of a given propellant, at a given initial temperature, u_{th} changes in accordance with changes in pressure. The following formulas sum up the adjusted experimental relationship for the use of u_{th} and p data obtained from multiple experiments.

87-1 $u_{th}=25+523.6/p$ m/s (20°C)

87-2 $u_{th}=(279.3/p^{0.1911})-142.3$ m/s (20°C)

From this relational formula, it can be seen that the higher the value of p, the lower the value of u_{th}, which is to say that under high pressures erosive burning is more likely to occur. The pressure range of the above formula is 3.43-11.08 MPa.

Thus when using the formula $\varepsilon=f(p,u)$, it is necessary first to find u_{th}, and only when $u\geq u_{th}$ to apply this formula.

Because the value r_{m0} is relatively low for propellant 87-2, r is relatively sensitive to fluctuations in u. In addition the propellant's charge base itself has an unstable rate of burning. The value of u_{th} is not very apparent, and the relative deviation in the formula defining the relations between u_{th} and p are somewhat larger.

4. Conclusions

The results discussed above yield the following conclusions:

(1) The increase in the erosion ratio ε for aluminized HIPB composite propellant 87 depends most importantly on the crosswise flow u and the pressure p. In the relationship $\varepsilon=f(p,u)$, $K_2<K_3$, which is to say that the influence of the rate of flow is the more important. This is even more apparent in the case of propellant 87-2, with its slow burning rate. The experimental relational formula that we have obtained is in accordance with regular patterns.

(2) For the influence of crosswise flow on the erosion ratio there exists a limiting rate value u_{th}. Especially in the case of propellant 87-2 with its low burning rate is u_{th} very low. For this reason, when designing the charge, it is necessary to pay attention to the size of the initial throat/passage ratio J; for example, for propellant 87-2, when p=5.88 MPa and $J\geq 0.2$, $\varepsilon_{calc}\geq 1.4$ and there appears a considerable level of erosive burning. In the case of propellant 87-1, however, with comparable p and J values, $\varepsilon_{calc}\leq 1.01$, or, in other words, there is basically no erosion.

(3) Composite propellant 87 does not exhibit a negative erosion phenomenon. In the process of u increasing from 0 to u_{th}, the ε value basically stays at 1.0. For this reason, the form $\varepsilon=1+K_1 p^{K_2} u^{K_3}$ is appropriate.

(4) The basic burning rate of propellant 87-2 is lower than that for 87-1. It is a slow-burning propellant, and the erosion effect should be stronger. The erosion ratio is larger, and the limiting flow rate u_{th} is smaller.

(5) For both propellants, 87-1 and 87-2, the results from the formula for erosive characteristics of propellant 87-1 and 87-2 are comparable to the

experimental values, and relatively close; especially in the case of 87-1, where deviation $\Delta = (\varepsilon_{actual} - \varepsilon_{calc})/\varepsilon_{actual}$, almost all values are within a 3% range. In the case of propellant 87-2, however, because the value of ε is very sensitive to changes in u, and the basic burning rate of the fuel is also unstable, the deviation is a little larger, with the Δ values for the most part being within the 5% range. This is basically the same as the manufacturer's expressed r_0 deviation. The experimental values and the calculated values are compared in Fig. 6 and Fig. 7.

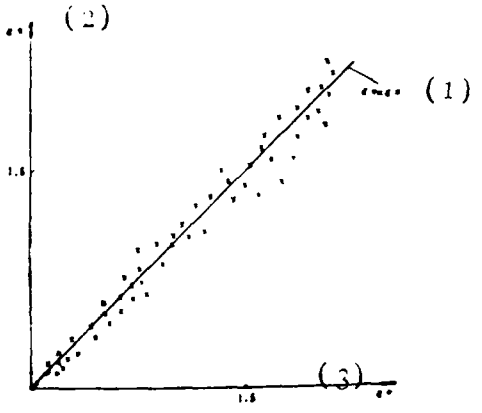

Fig. 6. Comparison of ε_{actual} and ε_{calc} for propellant 87-1. Key: (1) $\varepsilon_{actual}=\varepsilon_{calc}$; (2) ε_{actual}; (3) ε_{calc}.

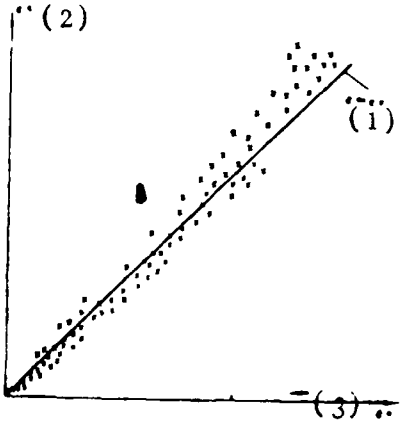

Fig. 7. Comparison of ε_{actual} and ε_{calc} for propellant 87-2. Key: (1) $\varepsilon_{actual}=\varepsilon_{calc}$; (2) ε_{actual}; (3) ε_{calc}.

BIBLIOGRAPHY

1. Razden, M.K. and K.K. Kuo. "Erosive burning study of composite solid propellants by turbulent boundary-layer approach," AIAA J. Vol. 17, 1979.

2. Razden, M.K. and K.K. Kuo. "Turbulent-flow analysis and measurements of erosive burning rates of composite solid propellants," AIAA 80-1209.

3. King, M.K. "Erosive burning of some composite solid propellants, experimental and modeling studies," Journal of Spacecraft and Rockets, Vol. 15, May-June 1979.

THE ACTION MECHANISM OF LEAD COMPOUNDS IN THE COMBUSTION PROCESS OF DOUBLE-BASE PROPELLANTS

Cai Yu Fang
(Beijing Institute of Technology)

Abstract

This paper proposes a mechanism for the reaction by which lead compounds catalyze the combustion of double-base propellants. It demonstrates that this kind of compound raises the combustion rate by raising the temperature gradients in the fizz zone on the combustion surface. The paper also proposes a new point of view, that lead compounds, by increasing the amount of carbonaceous matter on the combustion surface, increase the rate of combustion, and also, by reducing the carbonaceous matter, control the increase in combustion rate; it also proposes a reaction controlling the increase in carbonaceous matter, and explains the influence of pressure on this control capability. Finally, on the basis of the action mechanism proposed here and the principles of heat transfer, it explains the super-rate, plateau and mesa effects.

Key Terms: Double-base propellant, combustion catalyst of propellant, propellant combustion, incendiary effect.

1. Foreword

When a small amount of lead oxide products, or one of several inorganic or organic lead salts (the general name for which is lead series combustion rate catalyzers) have been added to a double-base propellant, a super-rate, plateau, and/or mesa effect is produced, causing the combustion rate characteristics to improve greatly. This kind of result has great practical significance for the design of solid fuel rocket motors and their reliable functioning. It is necessary to clarify the mechanisms in order to direct the

---

Translator's Notes:
Note in original: Paper received 10/14/86.
For bibliography, see page 34.

burning adjustments of solid propellants containing nitric acid esters and the study of low pressure index combustion rate catalysts.

Much experimentation and simulation work has been performed on this subject, both here and abroad. For the most important points and recent work on the subject, refer to the bibliography [1-9]. Nevertheless, plateau and mesa effects have not yet been explained, and the super-rate effect explanations are in need of improvement. For this reason, we have decided to undertake a comprehensive summary and study of the existing experimental phenomena and results that have a direct or indirect relationship with our subject. After we have established the basic reaction by which lead series combustion rate catalysts participate in the combustion process, we will combine it with the heat transfer principles to explain the super-rate, plateau, and mesa effects.

2. The Basic Reaction Causing Changes in Burning Rate

Often-used lead series combustion rate catalysts include oxidized lead products (as represented by lead oxide, lead carbonate, lead stearate, and lead salicylate), as well as inorganic lead salts and organic lead salts of fatty and aromatic acid. The stability of these lead salts under heat is higher than that of nitric acid ester. In the burning process after the nitric acid ester has broken down, they decompose and participate in the changing of the combustion speed in the form of small granules of lead oxide. The remaining components in the lead salts have a very great influence on the rate increase range and on the scope of the plateau and mesa region pressure.

A. Deposit and Growth of Carbon Products on the Combustion Surface

Experiment and observation [1, 7, 10, 11] show that after adding lead series combustion rate catalysts, carbon deposited on the burning surface increases, and the carbon layer deepens. It is thought that, because of the presence of lead oxide, a portion of the propellant decomposition products

HCHO, CHO, and $(CHO)_2$ change their reaction path, because experimentation shows that lead oxide can change the path of the decomposition of aggregate formaldehyde, and lower the temperature of decomposition, causing the carbon [11] and lead salt, produced by separation at 180°C, after reaching decomposition temperature, to be able to cause acetaldehyde to separate and produce carbon [14]. It is widely recognized that in the process of forming carbon black a chemical core action occurs first, and only then does the growth phase occur. Furthermore, the core reaction requires a much higher temperature than the growth [15, 16, 17]. From this it can be seen that in the process of forming the carbon deposit, the core action is the key step. Lead oxide has many actions in lowering the temperature for the above mentioned aldehyde decomposition, and in producing very many evenly distributed carbon nuclei. Consequently it causes the carbon deposit to increase and the carbon layer to deepen. The carbon deposit base on the combustion surface consists of the element carbon and also a small amount of hydrogen and hydroxyl, as well as other elements and groups. Very small lead oxide granules are thus pressed into the deposited carbon layer.

B. The Reduction Reaction of Nitric Oxide

The carbonaceous deposit on the combustion surface not only provides a fresh surface, but also a porous structure; on it are very many miniscule holes and grains with a diameter of 0.5 μ [10]. For this reason it has a relatively large surface area, as required by many reactions. The existence of the carbonaceous deposit changes a portion of the path for the reduction of nitric oxide, which does not undergo a high-activation energy reaction with carbon monoxide, but is reduced by the following reactions:

$$NO + 2C \longrightarrow C(N)_p + (O) \quad (1)$$

$$NO + C + C(H) \longrightarrow C(N)_p + C(OH) \quad (2)$$

$$NO + C + C(OH) \longrightarrow C(N)_p + C(OOH) \quad (3)$$

$$C(N)_p + C(N)_p \longrightarrow 2C + N_2 \quad (4)$$

$$C(O) \longrightarrow CO \quad (5)$$

$$C(COOH) \longrightarrow C(H) + CO_2 \quad (6)$$

In the reaction formulas, C represents carbon atoms in the surface carbonaceous deposit; $C(N)_p$ is nitrogen atoms adsorbed to the vicinity of the carbon; C(O), C(H), C(OH), and C(COOH) are oxygen atoms, hydrogen atoms, hydroxyl groups and carboxyl groups bonded on carbon. During the process of combustion, after nitric oxide in the carbonaceous deposit is split up, the neighboring adsorbed nitrogen quickly joins up into nitrogen molecules (reaction 4). The oxygen atoms then bonds on the surface carbon (reaction 1) and on the surface carbon that has hydrogen and the hydroxyl group (reactions 2 and 3). When the temperature of the carbonaceous deposit reaches about 900°C, the surface oxidized products are all transformed to CO (reaction 5) and CO_2 (reaction 6).

The reactions of nitric oxide on a carbohydrate surface at 305-450°C (see Watts [18]), as well as the results obtained by Levy and others [19], in passing a gas mixture composed of NO and He through a graphite bed maintained at a temperature of 494°C, demonstrate that at temperatures in this range NO is able to adsorb released ions and release a quantity of nitrogen gas corresponding to the amount of nitrogen contained in the ionized NO, and that the oxygen in it is adsorbed chemically over the carbon. For this reason, under conditions of the carbon deposit temperature on the surface of combustion and reacting gases in its vicinity, reactions (1) and (4) can take place. Consider the following: (1) On the carbon black granule surface and interior the existence of carbon-hydrogen bonds is beyond all doubt [20]; (2) the hydrogen on the carbon surface is active at room temperature and can be captured by bromine [21,22] and chlorine; (3) the existence of hydroxyl groups and carboxyl groups on the carbon surface is also beyond doubt [20], and furthermore the rate of production of hydroxyl and carboxyl groups on the fresh carbon surface by the bonds produced by the oxygen reaction has the greatest value at about 420°C; (4) the reaction H+NO OH+N is a link in the flame chain reaction H_2-NO [25,26]." From these experimental results and conclusions, it is possible to infer the existence of hydrogen bonds on the carbon deposit produced by components of the double-base propellant, and furthermore that reactions (2) and (3) can occur. Experimentation also shows that when the temperature exceeds 900°C, all the oxygen bonded on the carbon

is released in the form of CO [19]. The amount of CO_2 that is released in the action of the carbon black setting free its carboxyl groups is in agreement with the chemically established carboxyl group results [27]; when carbon black is heated to 800-1000°C, it sheds its oxygen-containing groups. From these observations it is inferred that the oxidized products on the surface of the carbon deposit, by reactions (5) and (6), are entirely transformed into CO and CO_2 at a temperature of about 900°C. In addition, Merryman and others [28] show in their experiments that the higher the temperature, the more rapid the reduction of NO on the carbon surface. When the carbon content of the coal ash bed used in the experiment is higher, the amount of NO that is reduced is greater.

3. The Reaction of Lead Oxide, Carbon, Nitric Oxide and Carbon Monoxide

Lead oxide is a strong oxidizer and it reacts easily with carbon and CO:

$$PbO + C \longrightarrow Pb + CO - 21.6 \text{ Kcal} \quad (7)$$

$$PbO + CO \longrightarrow Pb + CO_2 + 15.6 \text{ Kcal} \quad (8)$$

At 700°C reaction (7) proceeds rapidly; at 160-180°C, reaction (8) begins to occur [29]. When double-base propellants containing lead series combustion rate catalysts are burned, is possible to observe the presence of liquid lead droplets on the combustion surface and/or the upper surface of the carbon deposit [1, 10, 30].

3. Super-rate, Plateau and Mesa Effects

A. The Influence of Pressure on the Rate Increase Range

A result of the reduction of a portion of the NO by reactions (1)-(6) during the combustion process is that the reduction location migrates from the flame region to the carbon deposit and the reaction heat accordingly moves near the combustion surface and is released. Consequently the combustion surface fizz region's temperature gradient is raised and the rate of combustion is increased. The experimental results of Kubota support this

conclusion (refer to [31], Fig. 1, 3, 4). The deviation between the combustion rate range of propellants that have undergone the lead series combustion rate catalysis increase, in comparison with untreated propellants under the same conditions, is called the "rate increase range." The lead series combustion rate catalysts are able to increase the burning rate through an increase of the carbon deposit on the combustion surface. They are also able, through reaction (7), to reduce the carbonaceous deposit, even to the point of making it disappear entirely, to control the increase in burning speed. This kind of control action is greatly subject to the influence of pressure. For this reason there may appear on the burning rate-pressure graph regions in which the rate increase range decreases slowly as the pressure rises, and regions in which the rate increase range decreases sharply as the pressure rises.

The reaction temperature for reaction (7) is about 700°C; this is to say, only as long as the temperature of the lead oxide granules is lower than that value, can the carbon nuclei produced on their surface exist and increase. The temperature at the top of the carbon layer is the temperature (ca 900°C) at which the oxidation products on the surface of the carbon deposit are entirely transformed into CO and CO_2 (reactions [5] and [6]). Therefore, the maximum size of the carbon which can be deposited and grow is controlled by this temperature. During the burning process the lead oxide granules covered by the carbon deposit have a rate of temperature increase which is necessarily very much lower than when they have not been covered. For this reason, as the burning progresses, the area of contact between lead oxide and carbon has a temperature lower than that for the same reaction on the layer, and a delayed temperature differential arises. The reaction temperature for reaction (7) is about 200° lower than the carbon layer upper surface temperature. If there is not a delayed temperature differential the site for this reaction ought to be in the middle of the carbon layer; if there is a delayed temperature differential, the reaction may be postponed. When the delayed temperature differential is great, the reaction can even be held off for the upper surface of the carbon layer. When lead oxide granules have not been entirely covered by the carbonaceous layer (that is, the rate of covering has been reduced), it

is unlikely that a delayed temperature differential arise on the part of the lead oxide/carbon interface surface which is near the uncovered surface. For this reason the reactions on these interface surfaces (reaction [7] and subsequently reaction [8]), first occur in the carbonaceous layer. They assist each other (the former provides the reagents for the later, and the latter provides the reaction heat for the former), and quickly spread toward the internal interface surface. Their rate of expansion lowers in accordance with the carbon deposit rate of covering. On the interface surfaces on which delayed temperature differentials have not arisen, they expand and accelerate. As a result of the rapid advance of these two actions in the carbonaceous layer, portions of the deposited carbon, before reaching upper surface temperature, lose their heavy lead oxide carrier and subsequently are adsorbed from the combustion surface by the combustion gases. The result of these fragmentary carbon slices flying off the combustion surface is that a great loss of deposited carbon occurs on the burning surface, taking with it the reaction heat. As the covering rate of the deposited carbon decreases, the percentage of lost deposited carbon becomes high, and the percentage of the reaction heat removed is also high.

Reaction (7), through the reduction in the production of carbon deposits and the control by the covering rate of the burning rate increase, causes the rate increase range to decrease; but the pressure, through the temperature gradients of the reaction area, again controls this sort of control action. The reaction area temperature gradients, as the pressure rises, change precipitously. Under low pressure, the temperature gradients are small, and before the temperature of the lead oxide granules reaches 700°C, there is sufficient opportunity to produce carbon nuclei, and enough time for carbon deposits to grow. At this time, the presence of reaction (7) has very little influence on the amount of carbon deposit produced, even to the point of having no influence, and it is not possible to induce fragmentary carbon slices to fly off the burning surface and produce a loss in the amount of carbon deposit. Because under low pressure the restraining capability of reaction (7) is very weak, at times having no restraining action, the amount of carbon layer produced is great and the rate increase range is large. As

the pressure increases, the temperature gradients change sharply, and before the lead oxide granules' temperature reaches 700°C, the opportunity for producing carbon atoms is reduced and the time for producing carbon deposits is shortened. The amount of carbon deposit produced drops. Before the pressure rises to a certain value, the control action of reaction (7) only appears as a reduction in the carbon deposit produced as the pressure rises. For this reason the rate increase range gradually drops as the pressure rises. When the pressure is higher than a certain value, in addition to the continued reduction in the amount of carbon produced, the loss of carbon deposit increases because of the fragmentary carbon slices flying off the burning surface. For this reason, the rate increase range decreases rapidly as the pressure rises (because the control action of reaction [7] becomes rapidly stronger). Up until the time that the pressure increases to the point that temperature gradients are very steep and the pressure value is reached under which any carbon nucleus produced is immediately, without exception, oxidized by the lead oxide, the carbon deposit completely disappears, and the rate increase range is lowered to zero. From the photographs taken by Eisenreich (see [10], Figures 9, 10, 11), it is possible to see clearly that the amount of carbon deposit and the carbon layer thickness vary according to the pressure; under plateau-region pressure the fragmentary carbon slices leave the burning surface with a bright luminescence, while under the pressures at the very end of the plateau, this phenomenon no longer exists. The phenomenon which has been photographed offers an experimental foundation for our thesis of "the influence of pressure on the rate increase range." In addition, a small amount of carbon black or graphite added to double-base propellants containing lead series combustion rate catalysts is able to cause the plateau region position to migrate to a pressure region that is much higher than the original [32]. The explanation for this fact is that these carbon products assist in the formation and expansion of the delayed temperature differential, and accordingly reduce the restraining function of reaction (7).

B. The Production of Super-Rate, Plateau, and Mesa Effects

On the basis of what has preceded, although when the pressure is low the rate increase range is great, nevertheless, it is not in every pressure range that it is true that the lower the pressure, the greater the rate increase range. Because the limit to the amount of carbon deposited is controlled by the composition of the propellant, and because when the carbon layer is thick the positions in the carbon layer that have the most heat for reaction are far from the burning surface, the combustion rate/pressure graph shows an ideal pressure for the rate increase range reaching its highest value, and there appears a pressure region with an elevated pressure index. The super-rate effect is thus produced. When the propellant composition is different, the pressure range in which this effect appears shows great deviation. Some compositions do not show the super-rate effect under the ordinarily used experimental pressure range.

The reasons for the plateau and mesa effects are comparable. Both result from the restraining action of reaction (7) increasing greatly after the pressure has risen to a certain value, thus leading to the rate increase range dropping sharply as the pressure rises. The difference is only that in the mesa range the rate increase range drops even more swiftly as the pressure rises. If the combination of the rate increase range and the burning rate range (which increases with the pressure) over a given pressure range is maintained at a certain value or increases very little, the plateau effect occurs. If the combination of these two factors over a given pressure range decreases as the pressure rises, the mesa effect occurs (Fig. 1).

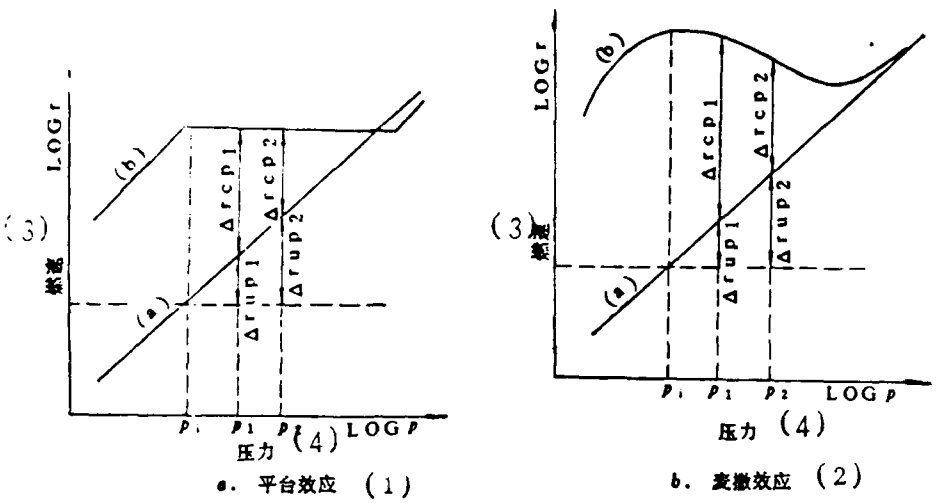

$$\Delta r_{cp_1}+\Delta r_{up_1}=\Delta r_{cp_2}+\Delta r_{up_2} \qquad \Delta r_{cp_1}+\Delta r_{up_1}>\Delta r_{cp_2}+\Delta r_{up_2}$$

Fig. 1. Origin of plateau and mesa effects. Key: (1) a. plateau effect; (2) b. mesa effect; (3) combustion speed; (4) pressure.

Notes to Figure 1: Both graphs represent double-base inorganic propellants containing lead series combustion rate catalysts. Δr_{cp1} and Δr_{cp2} are the rate increase ranges induced by the catalyst under pressures p_1 and p_2, respectively. Δr_{up1} and Δr_{up2} are the increases in the rate increase range resulting from the rise of pressure p_1 to p_1 and p_2, respectively.

BIBLIOGRAPHY

1. Kubota, N., T.J. Ohlemiller, L.H. Cavecy, and M. Summerfield. AD 763786, 1973.

2. Bing Qi Cheng Ye Bu 20 Yuan. "The current state abroad of double-base plateau propellant burning mechanisms," internal reference material, 1975.

3. Singh, H. and K.R.K. Rao. AIAA J., 15, 1545, 1977.

4. Wilmot, G.B., E.G. Powell, J. Sharma and D. Carlson. 18th JANNAF Combustion Meeting, CPIA Publication, 3, p. 297, 1981.

5. Singh, H. and K.R.K. Rao. IAF paper 82-395, 1982.

6. Ferreira, J.G., A. Bizot and G. Lengelle. AIAA paper 83-1197, 1983.

7. Duterque, J., L. Ommel and G. Lengelle. Propellants, Explos., Pyrotech., 10, 18, 1985.

8. Singh., H. and K.R.K. Rao. Adv. Catal. (Proc. Natl. Symp. Catal.), 7th, p. 229, 1985.

9. Singh., H. and K.R.K. Rao. Indian J. Technol., 24(1), 26, 1986.

10. Eisenreich, N. Propellants Explos., 3, 141, 1978.

11. Hewkin, D.J., J.A. Hicks, J. Powling and H. Watts. Combust. Sci. Technol., 2, 307, 1971.

12. Cohen, N.S., and G.A. Lo. AIAA paper 83-1198, 1983.

13. Lengelle, G., L. Deterque, C. Verdier, A. Bizot, and J.P. Trubert. 17th Symposium (International) on Combustion, The Combustion Institute, p. 1443, 1979.

14. Olson, D.B., D.G. Keil and H.F. Calcote. AD-A 146817, 1984.

15. Tesner, P.A. and A.I. Yecheistsva. Dokl. Akad. Nauk USSR, 87, 1029, 1952.

16. Tesner, P.A. Symp. Combust. 7th London, Oxford, p.546, 1959.

17. Tesner, P.A., M.M. Polyakova and S.S. Mikheeva. Tr. Vses. Nauk Issled. Inst. Pri. Gazov, 40/48, 8, 1969.

18. Watts, H. Trans. Faraday Soc., 54, 93, 1958.

19. Levy, J.M., L.K. Chan, A.F. Sarofim and L.M Beer. 18th Symposium (International) on Combustion, The Combustion Institute, p. 111, 1981.

20. Donnet, J.B. and A. Vost. Carbon Black, New York and Basel, 1976.

21. Lezhnev, N.N., A.P. Terentev, I.S. Novikova and T.A. Kobzeva. Sov. Rubber Technol., 9, 17, 1965.

22. Bochm, H.P., U. Hoffman and A. Claus. Proc. 3rd Conf. on Carbon, p. 241, 1965.

23. Puri, B.R. and R.C. Bansal. Indian J. Chem., 5, 381, 1967.

24. King, A. J. Chem Soc., 1489, 1937.

25. Mainiero, R.J. and Vanpee, M. Combust. Sci. Technol., 22, 171, 1980.

26. Magnus, A.U., P.S. Chintapalli and M. Vanpee. Combust. Flame, 22, 71, 1974.

27. Puri, B.R. and R.C. Bansal. Carbon, 1, 451, 1964.

28. Merryman, E.L., S.E. Miller and A. Levy. Combust. Sci. Technol., 20, 161, 1979.

29. Dong Bei Gong Xue Yuan You Se Jin Shu Ye Lian Jiao Yan Shi. "Lead Metallurgy" Ye Jin Gong Ye Chu Ban She [Metallurgical Industrial Press], p. 121, 1976.

30. Brown, L.M. and J.L. Chaille. Bulletin of 12th Meeting of the JANNAF Solid Propellant Group, 275, 1956.

31. Kubota, N. 17th Symposium (International) on Combustion, The Combustion Institute, 1345, 1978.

32. Preckel, R.F. AIAA J., 3, 346, 1965.

DISTRIBUTION LIST

DISTRIBUTION DIRECT TO RECIPIENT

ORGANIZATION	MICROFICHE
A205 DMAHTC	1
C509 BALLISTIC RES LAB	1
C510 R&T LABS/AVEADCOM	1
C513 ARRADCOM	1
C535 AVRADCOM/TSARCOM	1
C539 TRASANA	1
C591 FSTC	4
C619 MIA REDSTONE	1
D008 MISC	1
E053 HQ USAF/INET	1
E404 AEDC/DOF	1
E408 AFWL	1
E410 AD/IND	1
E429 SD/IND	1
P005 DOE/ISA/DDI	1
P050 CIA/OCR/ADD/SD	2
AFIT/LDE	1
FTD	
CCV	1
MIA/PHS	1
LLYL/CODE L-389	1
NASA/NST-44	1
NSA/T513/TDL	2
ASD/FTD/TQLA	1
FSL/NIX-5	1